

# LABEL PROPAGATION VIA RANDOM WALK FOR TRAINING ROBUST THALAMUS NUCLEI PARCELLATION MODEL FROM NOISY ANNOTATIONS

Anqi Feng<sup>1</sup>, Yuan Xue<sup>2</sup> Member, IEEE, Yuli Wang<sup>1</sup>, Chang Yan<sup>3</sup>,  
Zhangxing Bian<sup>2</sup>, Muhan Shao<sup>2</sup>, Jiachen Zhuo<sup>4</sup>, Rao P. Gullapalli<sup>4</sup>,  
Aaron Carass<sup>2</sup> Member, IEEE, and Jerry L. Prince<sup>1,2</sup> Fellow, IEEE

<sup>1</sup> Department of Biomedical Engineering, Johns Hopkins School of Medicine, USA

<sup>2</sup> Department of Electrical and Computer Engineering, Johns Hopkins University, USA

<sup>3</sup> Department of Information Technology and Electrical Engineering, ETH Zurich, Switzerland

<sup>4</sup> Department of Diagnostic Radiology and Nuclear Medicine,  
University of Maryland School of Medicine, USA

## ABSTRACT

Data-driven thalamic nuclei parcellation depends on high-quality manual annotations. However, the small size and low contrast changes among thalamic nuclei, yield annotations that are often incomplete, noisy, or ambiguously labelled. To train a robust thalamic nuclei parcellation model with noisy annotations, we propose a label propagation algorithm based on random walker to refine the annotations before model training. A two-step model was trained to generate first the whole thalamus and then the nuclei masks. We conducted experiments on a mild traumatic brain injury (mTBI) dataset with noisy thalamic nuclei annotations. Our model outperforms current state-of-the-art thalamic nuclei parcellations by a clear margin. We believe our method can also facilitate the training of other parcellation models with noisy labels.

**Index Terms**— Thalamic nuclei, MRI, 3D Unet, Label propagation, Random walk

## 1. INTRODUCTION

The thalamus is an essential relay station in the brain that passes information from peripheral nerves to the cortex [1] and also reflects multiple behavioral states [2]. The thalamus has a complicated structure, consisting of multiple functional clusters called *nuclei*. These nuclei serve a wide variety of neurological functions and are closely associated with many neural disorders such as schizophrenia, multiple sclerosis [3], Alzheimer’s disease, epilepsy, Huntington’s disease, and dyslexia [4] where both atrophy and functional changes can be observed. Therefore, accurate segmentation of the thalamus and thalamic nuclei can be helpful in clinical medicine.

Machine learning has proven successful at magnetic resonance (MR) based thalamic nuclei parcellation [5, 6]. However, such methods rely on high-quality thalamic nuclei annotations for model training. This is a difficult task in practice for sev-

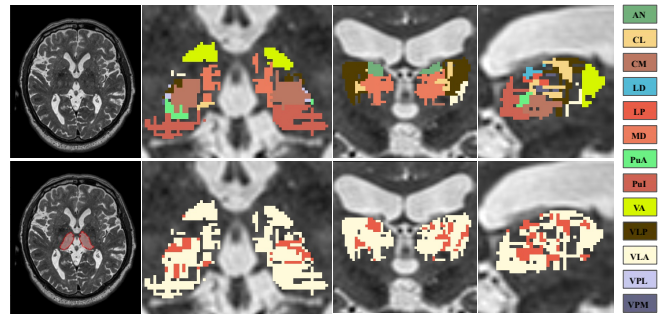


**Fig. 1.** A 3D T2 weighted MR image and its corresponding thalamus mask are shown in the first column. The next three columns are zoomed axial, coronal, and sagittal views, respectively. The top row has the thalamic nuclei labels (color key in the right-most column). The bottom row shows voxels with one label (79.8%) in white and multiple labels (20.2%) in red.

eral reasons [4, 7, 8]: 1) nuclei are small [9]; 2) low contrast between nuclei; 3) delineations done on 2D slices while the nuclei are 3D structures, and 4) independent labeling of separate nuclei can lead to gaps and overlaps—as shown in Fig. 1.

To leverage imperfect annotations, efforts have been made towards training models with noisy labels. Gao et al. [10] proposed a constrained segmentation propagation algorithm which uses information from sparse annotations and voxel-wise segmentation results from deep convolutional neural networks, and formulates it into a fully-connected conditional random field. However, the algorithm only works in 2D. Breve et al. [11] proposed a two-stage graph-based label propagation method, spreading “scribbles” to complete labels; this method may not be transferable to thalamus nuclei segmentation due to the low image contrast between nuclei.

In this paper, we propose a robust thalamic nuclei segmentation framework that can be trained with noisy, incomplete

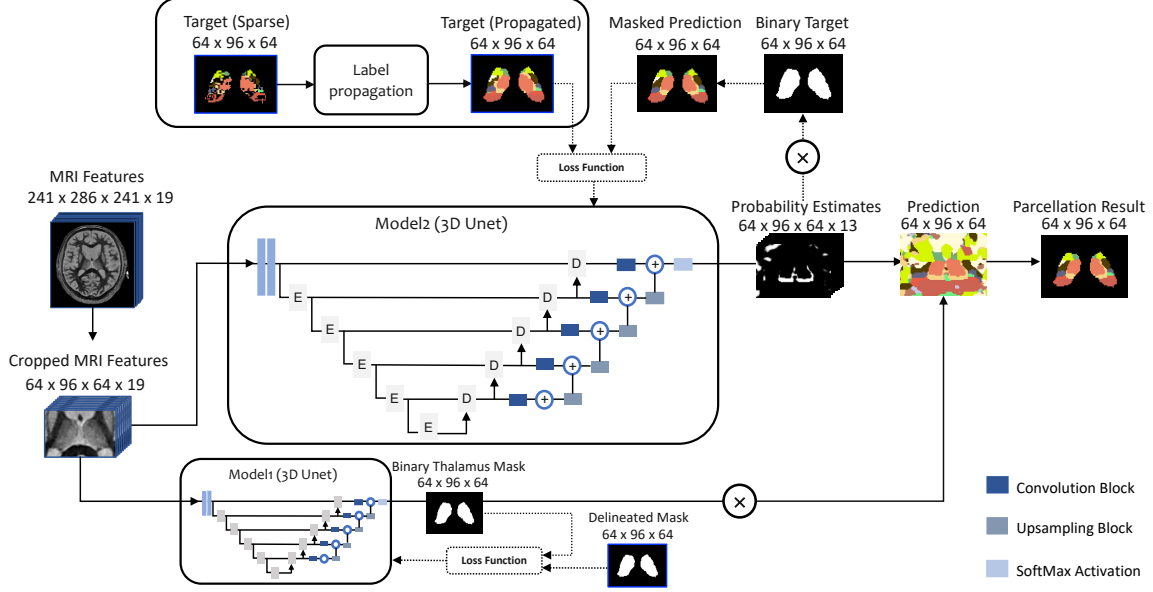


**Fig. 2.** An overview of the proposed model. The parcellation model takes 3D MRI volumes with 19 features as input and generates both a whole thalamus mask and thalamic nuclei labels. Two models are trained separately in a two-step way. The whole thalamus mask is applied to the thalamic nuclei labels to get the final parcellation result.

annotations. Given the original annotation, which may contain gaps and have multiple labels assigned to voxels, we remove all overlapping labels and perform a label propagation using the random walk algorithm on an edge map. The propagated whole thalamus mask and thalamic nuclei labels train a two-step parcellation network based on 3D Unet. The class imbalance issue due to the small nuclei sizes is mitigated by focusing only on the thalamus. Compared to Yan et al. [12] and a baseline method trained without label propagation, our proposed method achieves both quantitatively and qualitatively better performance.

## 2. METHODOLOGY

An overview of our thalamic nuclei parcellation framework is shown in Fig. 2; the following subsections provide a detailed description.

### 2.1. Label Propagation

As input, a manual delineation has thalamic voxels with no label, one label, or multiple labels. We start by setting all voxels with multiple labels as unlabeled. We next use the random walk algorithm [13] to propagate the remaining labels into unlabeled voxels within the thalamus, where labeled voxels are kept fixed. The random walk algorithm takes an input image, such as a magnetization-prepared rapid gradient-echo (MPRAGE) MR sequence, and forms the undirected graph  $G = (N, E)$ . The nodes,  $N$ , are the voxels of the image and the edges,  $E$ , denote the connection between two neigh-

boring nodes, in this case the six neighbors of a voxel. The edge,  $e_{ij}$ , between nodes  $i$  and  $j$  has weight:

$$w_{ij} = \exp(-\beta|g_i - g_j|^2),$$

where  $g$ 's are the intensity values of nodes ( $i$  or  $j$ ) and  $\beta$  is a hyperparameter. In our experiments, we will compare results that use intensities arising from different images: T1-map, MPRAGE, FGATIR [14, 15], and T2-weighted. Label propagation is formulated as a combinatorial Dirichlet problem [16] with desired random walker probabilities. The label propagation problem based on Dirichlet integral can be achieved by:

$$\arg \min_{\mathbf{X}} \frac{1}{2} \sum_{e_{ij} \in E} w_{ij} (\mathbf{x}_i - \mathbf{x}_j)^2,$$

where  $\mathbf{X}$  is a random field over  $\{\mathbf{x}_1, \dots, \mathbf{x}_n\}$ , with  $\mathbf{x}_i$  representing the probability that node  $i$  belongs to the label set  $\{l_1, \dots, l_m\}$ . After label propagation, the refined labels can be used to train the model introduced in Sec. 2.2 without needing hard label conversion. Qualitative results of label propagation based on random walk are shown in Fig. 3.

### 2.2. Thalamus Nuclei Parcellation

We first use a 3D Unet [17] to segment the whole thalamus, outputting a whole thalamus mask [18]. We then use a second 3D Unet to identify 13 classes corresponding to the 13 thalamic nuclei labels in each thalamic hemisphere. These 13 class predictions are then multiplied by the predicted whole thalamus mask to get the final thalamic nuclei masks.

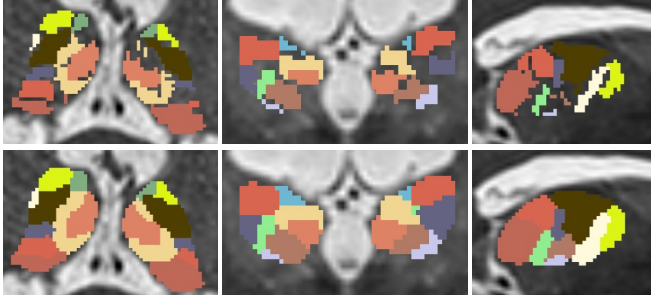


**Fig. 3.** Label propagation results. Top: Original noisy labels overlaid on 3DT2 weighted. Bottom: Propagated labels overlaid on 3DT2 weighted. Left to right are axial, coronal, and sagittal views. All the images come from the same subject.

During the training of the second network, we only calculate the loss inside the thalamus to avoid the class imbalance issue that would otherwise arise from background voxels. For comparison, we trained the second network in two ways. As a baseline method, we trained the network using only the original annotations. Since these annotations contain voxels with multiple labels, we converted the labels into membership vectors where a voxel with  $n$  labels assigns  $1/n$  membership to each label. The network was trained with cross-entropy to produce 13 thalamic nuclei class labels. We also trained the second network using the propagated labels and a Dice loss.

### 3. EXPERIMENTS AND RESULTS

**Dataset** For both training and testing, we used MR scans from 30 subjects. For each subject, multi-contrast MR features, including fast gray matter acquisition T1 inversion recovery (FGATIR) [14], MPRAGE, three-dimensional T2-weighted (3D-T2w), T1 map, and diffusion tensor imaging (DTI) were available. The DTI data were used to generate diffusion measures, including fractional anisotropy (FA), mean diffusivity (MD), axial diffusivity (AD), radial diffusivity (RD), trace (Tr), 3 Westin Indices (3WI), mode, eigenvectors, and eigenvalues. Eigenvectors and eigenvalues were further used to construct the 5D Knutsson vector and edge map [19]. All images were registered to the MPRAGE, non-directional images were normalized to the range of  $[0, 1]$ , while directional features were normalized to  $[-1, 1]$ . We also perform center-cropping to crop the images from  $241 \times 286 \times 241$  to  $64 \times 96 \times 64$ . The MPRAGE, FGATIR, 3D-T2, T1 map, FA, MD, AD, RD, Tr, 3WI, mode, and the 5D Knutsson vector and edge map were combined into a 19-dimensional feature vector.

The 30 subjects were semi-automatically annotated using the following steps: 1) the Morel atlas [7] was affinely registered to a subject's MPRAGE image; 2) the atlas labels were individually transformed into the subject's space, which can lead to discontinuities and label overlaps; 3) atlas labels were

reviewed and manually corrected, this correction (as shown in Fig. 1) does not resolve the label gaps and overlaps. The nuclei used in this work are the: anterior nucleus (AN), central lateral (CL), center median (CM), lateral dorsal (LD), lateral posterior (LP), mediodorsal (MD), anterior pulvinar (PuA), inferior pulvinar (PuI), ventral anterior (VA), ventral lateral anterior (VLA), ventral lateral posterior (VLP), ventral posterior lateral (VPL), ventral posterior medial (VPM).

Our baseline Unet method refers to Unet trained with the original (noisy) labels. We also trained four more Unets using propagated labels from the random walk algorithm where  $\beta$  is 10,000 and used the T1 map, MPRAGE, FGATIR, and 3D-T2w images as the edgemap. For this, we did a 10-fold cross validation with 25 training, 2 validation, and 3 testing subjects in each fold. For the Unet training, we used the SGD optimizer with an initial learning rate of  $5 \times 10^{-2}$ , which decreased by 10% every 20 epochs, and a momentum of 0.9. The models were trained for 200 epochs. During evaluation, we excluded voxels with ambiguous annotations on the testing data and calculate the Dice coefficient of the prediction multiplied by the binary version of target. We calculated Dice for each thalamus nuclei class and report a volume-weighted mean of the Dice score for each of the 13 classes (Table 1).

The results in Table 1 show clear improvement over the previously reported method of Yan et al. [12]. The Yan method used the same 19 features that we use here and then applied the UMAP [20] method followed by  $k$  nearest neighbors (KNN) in the resulting 2D space. Among the Unet methods, we observe overall best performance with the propagated labels from the MPRAGE image. Individual nuclei may favor a particular contrast, but these differences are mostly small. Only the VLA shows better results when using the baseline UNet.

Qualitative thalamic nuclei parcellation results are shown in Fig. 4. We observe that each variation of our proposed method achieves better performance than Yan et al. [12]. Most nuclei segmented using models with propagated labels show higher concordance with the target delineation than the baseline method. For example, the central lateral nucleus (CL) class, as highlighted by the blue circle, is clearly predicted by UnetT1, UnetT2w and UnetMP, while the baseline Unet predicts it as MD. However, the ventral lateral anterior nucleus (VLA) class, as highlighted by the purple arrows, appears visually better in the baseline Unet than UnetT1 and UnetT2w, both of which predict the VLA class as VLP.

### 4. CONCLUSION

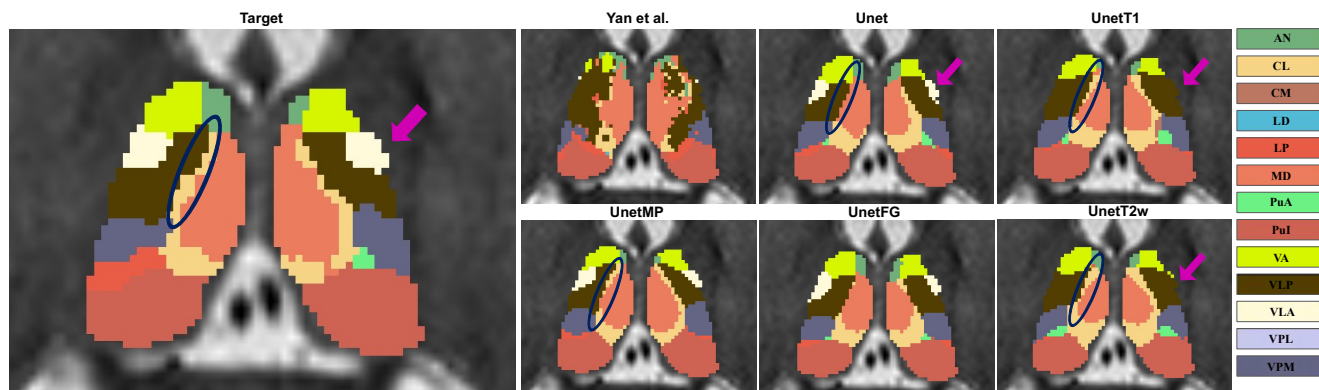
In this paper, we proposed a thalamic nuclei parcellation model which can be trained with noisy annotations. A random walk based label propagation was used to refine the original annotations with conflicting and missing voxels. Compared with existing models and a baseline Unet model trained with the original labels, our proposed model trained with our propagated labels achieved better performance, both quantitatively

**Table 1.** Dice score of the 10-fold cross-validation experiment. The ‘‘Overall’’ label is a volume weighted combination of the thirteen Dice scores. Dice score is expressed as a percentage. **Key:** Yan et al. - A comparison method that uses UMAP to reduce 19D data features (either to 2D, 3D, or 4D), followed by KNN to perform voxel-wise classifications; Unet - Unet with noisy labels; UnetT1 - Unet with propagated labels using T1 map; UnetMP - Unet with propagated labels using MPRAGE; UnetFG - Unet with propagated labels using FGATIR; UnetT2w - Unet with propagated labels using 3D T2 weighted images.

Method	Overall	AN	CL	CM	LD	LP	MD
<b>Yan et al.</b>	60.33 ± 4.06	21.08 ± 10.06	32.37 ± 6.78	32.85 ± 5.12	0.74 ± 0.08	46.20 ± 5.54	72.81 ± 3.60
<b>Unet</b>	87.10 ± 8.19	82.24 ± 11.94	68.94 ± 10.56	78.48 ± 10.56	52.34 ± 21.92	86.28 ± 8.02	92.91 ± 6.70
<b>UnetT1</b>	88.70 ± 7.56	85.99 ± 9.07	70.25 ± 12.99	<b>85.79 ± 8.75</b>	57.87 ± 24.35	88.42 ± 7.93	<b>93.45 ± 4.51</b>
<b>UnetMP</b>	<b>88.95 ± 6.37</b>	<b>89.32 ± 7.50</b>	71.33 ± 10.25	84.08 ± 8.38	<b>58.40 ± 31.93</b>	<b>89.79 ± 5.68</b>	93.44 ± 4.87
<b>UnetFG</b>	88.89 ± 5.86	88.80 ± 6.22	70.78 ± 9.26	85.19 ± 4.69	55.11 ± 31.19	86.96 ± 8.57	93.32 ± 4.03
<b>UnetT2w</b>	87.87 ± 7.18	88.28 ± 10.55	<b>71.98 ± 9.25</b>	84.26 ± 6.78	41.08 ± 34.83	86.60 ± 7.83	92.61 ± 3.85

Method	PuA	PuI	VA	VLP	VLA	VPL	VPM
<b>Yan et al.</b>	8.29 ± 6.10	86.82 ± 2.27	66.22 ± 4.24	61.98 ± 3.10	15.45 ± 6.95	37.79 ± 5.07	35.66 ± 6.42
<b>Unet</b>	48.78 ± 20.65	97.31 ± 2.74	89.26 ± 13.97	89.44 ± 6.59	<b>72.38 ± 17.54</b>	77.44 ± 12.96	66.23 ± 23.94
<b>UnetT1</b>	57.49 ± 19.83	97.67 ± 1.99	93.10 ± 4.67	89.92 ± 9.69	68.58 ± 28.92	81.14 ± 9.81	71.93 ± 18.88
<b>UnetMP</b>	54.42 ± 18.58	97.60 ± 2.01	93.96 ± 4.31	92.41 ± 4.01	53.01 ± 33.34	81.19 ± 7.86	67.25 ± 27.73
<b>UnetFG</b>	50.76 ± 20.53	<b>97.81 ± 2.12</b>	94.83 ± 3.92	<b>92.51 ± 3.40</b>	50.83 ± 35.80	<b>81.55 ± 8.44</b>	75.25 ± 13.11
<b>UnetT2w</b>	<b>58.46 ± 14.94</b>	97.60 ± 1.98	<b>95.09 ± 4.01</b>	88.88 ± 9.47	46.02 ± 34.03	79.33 ± 11.55	<b>78.91 ± 13.59</b>



**Fig. 4.** Qualitative comparison of different parcellation results. The target after label propagation and parcellation results are shown respectively. The target is a label fusion result of the propagated labels calculated based on T1 map, MPRAGE, FGATIR, and 3DT2 weighted using majority voting implemented from: <https://github.com/FETS-AI/LabelFusion>.

and qualitatively. We believe our proposed model can be extended to other medical imaging applications where noisy annotations are common.

## 5. ACKNOWLEDGMENTS

This work was supported in part by the NIH through the National Institute of Neurological Disorders and Stroke (NINDS) grant R01-NS105503 (PI: R.P. Gullapalli). The data was acquired in line with the principles of the Declaration of Helsinki. Approval was granted by an IRB Committee of the University of Maryland School of Medicine.

## References

- [1] S. M. Sherman and R. W. Guillery, *Exploring the thalamus and its role in cortical function*, MIT press, 2006.
- [2] S. M. Sherman and R. W. Guillery, ‘‘The role of the thalamus in the flow of information to the cortex,’’ *Philosophical Transactions of the Royal Society of London. Series B: Biological Sciences*, vol. 357, no. 1428, pp. 1695–1708, 2002.
- [3] J. Glaister et al., ‘‘Thalamus Segmentation using Multi-Modal Feature Classification: Validation and Pilot Study of an Age-Matched Cohort,’’ *NeuroImage*, vol. 158, pp. 430–440, 2017.
- [4] J. E. Iglesias et al., ‘‘A probabilistic atlas of the human

- thalamic nuclei combining ex vivo MRI and histology,” *NeuroImage*, vol. 183, pp. 314–326, 2018.
- [5] J. V. Stough et al., “Automatic method for thalamus parcellation using multi-modal feature classification,” in *International Conference on Medical Image Computing and Computer-Assisted Intervention*. Springer, 2014, pp. 169–176.
- [6] U. Ziyan et al., “Segmentation of thalamic nuclei from DTI using spectral clustering,” in *International Conference on Medical Image Computing and Computer-Assisted Intervention*. Springer, 2006, pp. 807–814.
- [7] K. Niemann et al., “The Morel stereotactic atlas of the human thalamus: atlas-to-MR registration of internally consistent canonical model,” *NeuroImage*, vol. 12, no. 6, pp. 601–616, 2000.
- [8] J. H. Su et al., “Thalamus Optimized Multi Atlas Segmentation (THOMAS): fast, fully automated segmentation of thalamic nuclei from structural MRI,” *NeuroImage*, vol. 194, pp. 272–282, 2019.
- [9] S. S. Keller et al., “Volume estimation of the thalamus using FreeSurfer and stereology: Consistency between methods,” *Neuroinformatics*, vol. 10, no. 4, pp. 341–350, 2012.
- [10] M. Gao et al., “Segmentation label propagation using deep convolutional neural networks and dense conditional random field,” in *2016 IEEE 13th International Symposium on Biomedical Imaging (ISBI)*. IEEE, 2016, pp. 1265–1268.
- [11] F. Breve, “Interactive image segmentation using label propagation through complex networks,” *Expert Systems With Applications*, vol. 123, pp. 18–33, 2019.
- [12] C. Yan et al., “Segmenting thalamic nuclei from manifold projections of multi-contrast MRI,” in *Proceedings of SPIE Medical Imaging (SPIE-MI 2023)*, San Diego, CA, February 19 – 23, 2023. SPIE, 2023.
- [13] L. Grady, “Random walks for image segmentation,” *IEEE Trans. Patt. Anal. Mach. Intell.*, vol. 28, no. 11, pp. 1768–1783, 2006.
- [14] A. Sudhyadhom et al., “A high resolution and high contrast MRI for differentiation of subcortical structures for DBS targeting: FGATIR,” *NeuroImage*, vol. 47, no. S2, pp. T44–T52, 2009.
- [15] P. Tohidi et al., “Multiple Sclerosis brain lesion segmentation with different architecture ensembles,” in *Proceedings of SPIE Medical Imaging (SPIE-MI 2023)*, San Diego, CA, February 19 – 23, 2023, 2023.
- [16] N. Biggs, “Algebraic potential theory on graphs,” *Bulletin of the London Mathematical Society*, vol. 29, no. 6, pp. 641–682, 1997.
- [17] Ö. Çiçek et al., “3D U-Net: learning dense volumetric segmentation from sparse annotation,” in *International conference on medical image computing and computer-assisted intervention*. Springer, 2016, pp. 424–432.
- [18] M. Shao et al., “Evaluating the impact of MR image harmonization on thalamus deep network segmentation,” in *Proceedings of SPIE Medical Imaging (SPIE-MI 2022)*, San Diego, CA, February 20 – 24, 2022. SPIE, 2022, vol. 12032, pp. 115–121.
- [19] H. Knutsson, “Producing a continuous and distance preserving 5-D vector representation of 3-D orientation,” in *IEEE Computer Society Workshop on Computer Architecture for Pattern Analysis and Image Database Management*, 1985, pp. 175–182.
- [20] L. McInnes et al., “UMAP: Uniform Manifold Approximation and Projection,” *The Journal of Open Source Software*, vol. 3, no. 29, pp. 861, 2018.